Assembled Monolayer Nanorod Heterojunctions

Jessy B. Rivest,[†] Sarah L. Swisher,[‡] Lam-Kiu Fong,[§] Haimei Zheng,[⊥] and A. Paul Alivisatos[§,⊥,*]

[†]Department of Mechanical Engineering, [‡]Department of Electrical Engineering, and [§]Department of Chemistry, University of California, Berkeley, California 94720, United States, and [⊥]Materials Science Division, Lawrence Berkeley National Laboratory, Berkeley, California 94720, United States

ABSTRACT Compositional and interfacial control in heterojunction thin films is critical to the performance of complex devices that separate or combine charges. For high performance, these applications require epitaxially matched interfaces, which are difficult to produce. Here, we present a new architecture for producing low-strain, single-crystalline heterojunctions using self-assembly and in-film cation exchange of colloidal nanorods. A systematic set of experiments demonstrates a cation exchange procedure that lends precise control over compositional depths in a monolayer film of vertically aligned nanorods. Compositional changes are reflected by electrical performance as rectification is induced, quenched, and reversed during cation exchange from CdS to Cu_2S to PbS. As an additional benefit, we achieve this single-crystal architecture *via* an inherently simple and low-temperature wet chemical process, which is general to a variety of chemistries. This permits ensemble measurement of transport through a colloidal nanoparticle film with no interparticle charge hopping.

KEYWORDS: cation exchange · self-assembly · epitaxial heterojunction nanorod

A dense array of perpendicularly aligned but asymmetric semiconductor nanorods with a compositional change along the rod length is desirable for a variety of systems where charge separation across an interface is a first step: catalytic systems, sensors, light-emitting diodes, photovoltaics, and optoelectronics. Building upon work by others,[1−4] we have recently shown that colloidal semiconductor nanorods of a single composition can be organized by controlled evaporation over a reasonable length scale for device characterization.[5] However, the next step in producing such films with broken symmetry poses a challenge. While colloidal nanorods can be made asymmetric in solution by exploiting the different reactivity of the facets of a low-symmetry crystal during cation exchange,[6] it is still difficult to subsequently organize the asymmetric nanorods such that they will all point in the same direction. Evaporative assembly will not be selective; introduction of a chemically selective agent on the substrate may produce asymmetric alignment but will also likely block the subsequent charge flow pathways. Here we demonstrate that it is possible to create the desired asymmetric film by first assembling the single composition nanorods in an array and then performing cation exchange on that film (Figure 1). The ion exchange can be controlled to a high degree, affording a powerful means of patterning the nanorod films for subsequent use.

Cation exchange can be used to chemically convert the top layer of a crystalline film by replacing one cation for another while the anionic sublattice remains intact. However, the conversion is uneven in polycrystalline films, as the rate of exchange along different crystal axes can vary widely.[7,8] Columnar polycrystalline films yield improved uniformity but contain grain boundaries down which cations can travel and plate out, causing shunting, shorting, and cation deficiency.[9,10] In single crystals, cation exchange results in high interfacial strain, causing dislocations that act as performance-degrading recombination sites. Cation exchange in vertically oriented arrays of single-crystalline nanorods can relieve many of these challenges. The characteristic length over which dislocations are formed to relieve lattice mismatch are 5 nm or greater in many materials systems.[9,11] If the nanorod diameter is less than 5 nm, dislocations are avoided altogether and we reap only the benefits of ion exchange in a single crystal.

Recently, cation exchange has been applied to nanocrystals, in which this process has been shown to be uniquely shape-preserving and reversible, with reactions happening more rapidly than in the bulk and yielding high-quality material.[6,11−13] Here, we develop a new strategy to address the problem of *asymmetric*, single-nanocrystal cation exchange. We first fabricate a controlled structure using self-assembly and then use ion exchange to produce an array of oriented nanorod heterojunctions: In a vertically aligned, close-packed superlattice of nanorods on a substrate, ion access is limited to only the top end of

* Address correspondence to alivis@berkeley.edu.

Received for review January 14, 2011 and accepted April 6, 2011.

Published online April 06, 2011
10.1021/nn2001454

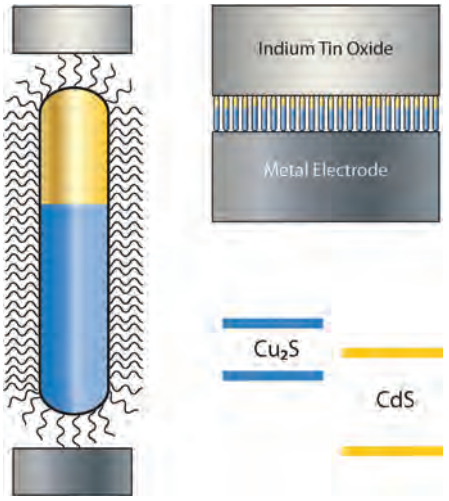

Figure 1. Schematic of parallel nanodiode or nanophotodiode arrays, and the bulk energy band alignment of our material system. Self-assembled colloidal CdS nanorods are partially converted (top ends only) to Cu_2S using our in-film cation exchange procedure.

individual nanorods, ensuring that exchange happens from only one end of the nanorod and that all nanodiodes are oriented in the same direction.

Here, cation exchange was performed *in film* by soaking the aligned nanorod film in a methanolic salt solution of the relevant cation in a dry, inert atmosphere. The molar amount of Cu^+ in the exchange solution was adjusted based on the number of required Cd^{2+} ion replacements to achieve exchange to a desired spatial depth into the aligned monolayer (Figure 2). It was assumed that the reaction went to completion (all Cu^+ ions went into nanorods).

The depth of the Cu exchange into the nanorod monolayer was characterized by Rutherford backscattering spectroscopy (RBS). Briefly, substrates were bombarded with He^{2+} ions. The kinetic energy of ions scattered elastically from the nanorod film were measured. Heights of Cd and Cu peaks in the RBS spectra allowed determination of the average film composition. Shifts in the peaks from their standard positions allowed approximate depth profiling of Cu- and Cd-rich sections (Figure 2c,d). Spectra confirm that Cu^+ exchange occurs selectively from the top end of aligned nanorods.

Further evidence for one-sided exchange is provided by transmission electron microscopy (TEM). By redispersing a film of aligned and cation-exchanged nanorods in chloroform and depositing the rods on an ultrathin carbon TEM grid, we were able to collect high-resolution TEM (HRTEM) and energy-filtered TEM (EFTEM) images to confirm asymmetric cation exchange. Studies of redispersed nanorods must be interpreted with care because they inevitably will include rods that had been standing (one end exposed) as well as some rods that stood along cracks in the film or lay flat on the substrate (both ends exposed) and

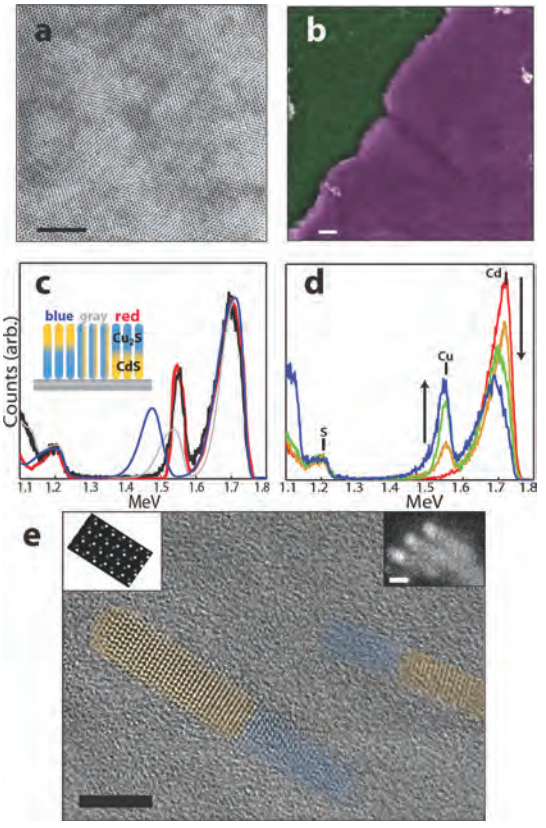

Figure 2. Self-assembled and cation-exchanged nanorod arrays. (a) Transmission electron microscopy (TEM) image of aligned nanorod array. (b) SEM false-color image of a film edge in a nanorod array, showing a monolayer of aligned rods (pink) on ITO (green). Scale bars are 100 nm. (c) Rutherford backscattering spectroscopy (RBS) demonstrates the selective copper ion exchange from the exposed ends of rods, resulting in asymmetry. Data (black) are fit with a simulated curve based on compositional depths (cartoon, inset). Simulations plotted show Cu_2S on top of CdS (red), Cu_2S and CdS evenly mixed within the film (gray) and Cu_2S underneath the CdS layer (blue). (d) RBS shows that the extent of cation exchange can be controlled. The shift to lower energies of the Cd peak as the film is further Cu^+-exchanged indicates that the Cd is in the bottom layer of the film. Correspondingly, the lack of a shift in the Cu peak indicates that Cu is restricted to the top layer of the film. No exchange (red), 20% exchange to Cu (orange), 40% (green), and 60% (blue). (e) High-resolution TEM (HRTEM) image showing an example heterojunction after redispersion. Left inset shows the simulated CdS structure, providing evidence that the higher-contrast portion of the rod is CdS, while the lower-contrast portion of the rod is the lower-symmetry Cu_2S. Right inset shows energy-filtered TEM image of redispersed nanorods, with the energy filter positioned at the Cu-M_1 edge. Scalebars in panel e are 5 nm.

some rods from the bottom of a multilayer (neither end exposed). However, the presence of significant numbers of nanorods with contrast profiles like those shown in Figure 2e is strongly suggestive of exchange that initiates on the exposed end of the rod film and propagates inward, with little or no exchange from the sides or buried ends of the rods. Extensive studies on HRTEM imaging of CdS−Cu_2S nanorods have shown that CdS is less sensitive to electron beam damage and appears to be higher in contrast compared with the counterpart of

Cu_2S within a nanorod (Figure 2e). HRTEM images depict the Cd−S dumbbell characteristic of wurtzite cadmium sulfide (higher contrast, shaded yellow). Cu minor edge EFTEM images (Figure 2e right inset) were collected with a filter set at 120 eV using a slit width of 5 eV. The bright portions of the nanorods suggest a non-uniform composition and can be interpreted, following ref 6, as the Cu_2S phase.

This method for producing asymmetric nanoparticles allows us to control the spatial depth of the exchange to Cu_2S systematically. Nanorods in the film can also be exchanged to Ag_2S[12] (Supporting Information) or, by use of a sequential cation exchange method, they can be double-exchanged to rock salt PbS.[14] The method may be generalized to the exchange of chalcogenides with various cations (HgS, Ag_2S, SnS_2, CdS, CdSe, ZnS, ZnSe Cu_2S, Bi_2S_3, and Sb_2S_3).[11,13,15,16]

A careful approach was required in order to make electrical contacts for studies of transport through these monolayer films. Evaporated metals have been employed successfully on relatively thick films or long nanowires,[17,18] but it has been shown that evaporation onto small nanorods can result in metal diffusion into the nanocrystal, altering electrical properties.[19] Further, evaporated metals may penetrate these thin films and produce shorts that can fluctuate in time, as in electrical measurements through monolayer molecular films.[20] In order to avoid shorting and damage to the nanocrystals, we made electrical contact using a room-temperature liquid metal (EGaIn) on a micromanipulator probe.[21] Approximate contact areas were measured with a side-view camera and ranged from a few to hundreds of micrometers in diameter (contacting 10^6−10^9 nanorods). All measurements were taken inside an argon glovebox at room temperature.

In order to demonstrate the high degree of compositional control provided by in-film cation exchange, we took electrical measurements of a monolayer film during a series of sequential cation exchanges on the same film (Figure 3). The chemical composition after each cation exchange step was confirmed using energy-dispersive X-ray spectroscopy in a scanning electron microscope (Supporting Information). The film region probed and the measurement conditions were kept approximately constant throughout. Measurements were repeatable in high-quality (well aligned monolayer) regions of the film over multiple cycles and multiple days, provided biases applied were no larger than ±0.5 V.

The initial CdS nanorod array (contacted by EGaIn and indium tin oxide (ITO)) showed a linear current−voltage shape characteristic of Ohmic contact, as expected based on previous work.[22,23] After partial (to a depth of 25% into the monolayer) exchange to Cu_2S, rectification was observed, as expected from a type II heterojunction.[24] At only 25% exchange, it is

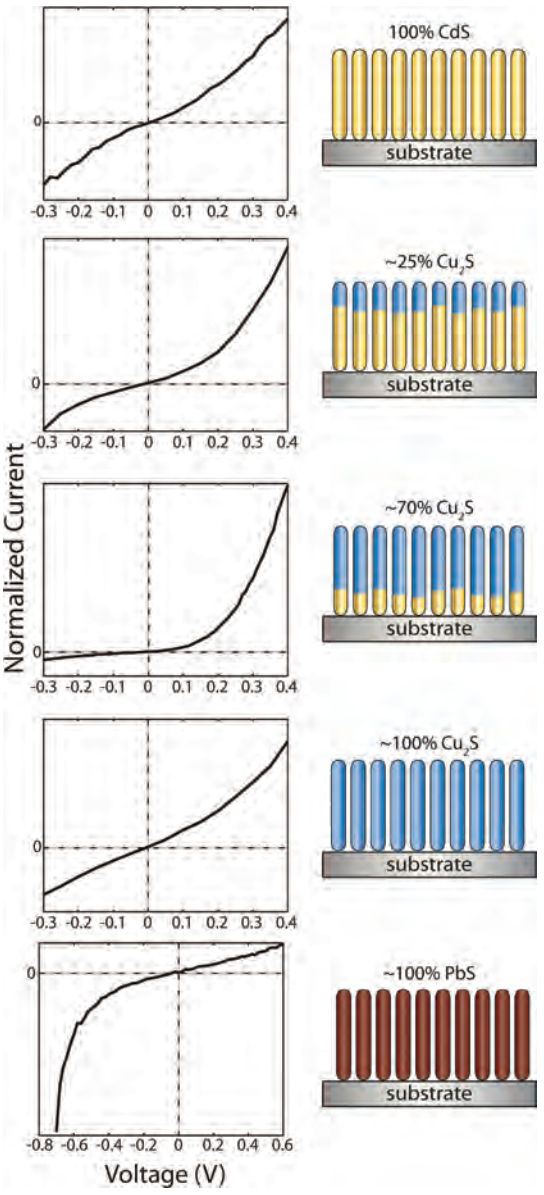

Figure 3. Sequential cation exchange. One film was used for a series of sequential cation exchanges: starting with CdS vertically aligned rods, Cu^+ was exchanged for Cd^{2+} to a 25% depth, then a 70% depth, then a 100% depth. Next, the resulting Cu_2S nanorods were exchanged fully to PbS. Between each cation exchange reaction, electrical measurements were taken and energy-dispersive X-ray spectra were collected to verify the chemical composition. In the last stage (bottom frame), the liquid metal top contact formed a Schottky junction with the PbS film, reversing the direction of rectification. All electrical measurements were performed in the dark.

likely that a fraction of the nanorods in the array are left unexchanged and provide a shunt path, limiting the rectification. Additionally, the high resistivity of CdS may increase series resistance in the diode, further reducing sharp rectification. From previous work,[6] it is expected that asymmetry in cation exchange from one nanorod end to another (001 to 00$\bar{1}$) does not exceed ~25%. Therefore, we expect that nanorods are exchanged with an average depth

uniformity of ±4 nm, in qualitative agreement with the RBS and TEM data.

Upon further soaking of the same film in a fresh and more concentrated cation solution to achieve ~70% cation exchange, the film showed greater rectification. This may be due to the formation of a Cu_2S top layer extending over the entire film, preventing shunts. Greater rectification may also be related to the reduction in the percentage of high-resistivity (CdS) semiconductor.

Further exchange of this film with an excess molar amount of Cu^+ resulted in a film fully exchanged to Cu_2S, which showed an Ohmic electrical response. Because Cu_2S is highly doped in the bulk by copper vacancies,[25] it screens electric fields efficiently, leading to short depletion regions which enable easy charge carrier tunneling through potential barriers.[26] Cu_2S is therefore expected to form Ohmic contact to most metals. In films of *unaligned* nanorods, no level of Cu^+ cation exchange produced rectification, most likely because the exchange results in a mixed-phase film with no common electric field to drive electrons toward the same electrode.

Following full sequential exchange from Cd^{2+} to Cu^+ and then to Pb^{2+} by soaking the Cu_2S film in a Pb^{2+} cation solution with a 10× molar excess of cations, the rectification direction reversed, as the resulting PbS rods formed Schottky junctions with the EGaIn probe. It is known that similarly quantum confined PbS forms a Schottky junction with aluminum,[27] and the near-equality of aluminum and EGaIn work functions (~−4.3 eV) suggests that the nature of the electrical contact may be the same. This series of experiments demonstrates precise control of composition and rectification of a nanorod film, using simple solution processing *in situ*.

The exchanged diodic films—both Cu_2S–CdS and PbS—showed a photoresponse when illuminated with AM1.5G solar flux (Figure 4). The photoresponse of the devices was stable (after exposure to air and subsequent storage in an argon glovebox) for more than 3 months and was repeatable over this time frame. The 30 nm long rods (and therefore 30 nm thick films) absorb approximately 8% of the solar spectrum above the Cu_2S and PbS confined band gaps. The types of nanocrystals studied here are currently being examined in a variety of quantum confined semiconductor photovoltaics, where interparticle hopping plays a key role in the transport.[17,27,28] In the monolayer devices studied here, there is no interparticle hopping, allowing the influence of contacts and intraparticle recombination to be separately investigated from hopping phenomena. The photovoltages produced by these devices are rather low (0.13 V for Cu_2S–CdS, and 0.15 V for PbS) compared with their theoretical values (~0.8 V for Cu_2S–CdS,[29,30] and ~0.4 V for PbS[14]) or their practical values (~0.45 V for Cu_2S–CdS,[31] and ~0.3 V for PbS[27]). The low photovoltage could be the result of a number of effects. In traditional photovoltaic devices, a low photovoltage is commonly associated with high recombination.[32] Given the high surface area of this system, it is reasonable to expect that there may be high rates of recombination that lower the photovoltage, and that these recombination sites could be passivated through ligand exchange or capping strategies. Alternatively, the low voltage could be a result of band alignments in the nanodiodes that differ from those observed in the bulk; quantum confinement and doping levels could cause large changes, as could pinning of the Fermi level. Other performance limitations may be set by the series resistance from the 1.8 nm insulating ligands or by fundamental problems with ultrathin heterojunctions, such as field quenching.[9,33] In future studies where the nanorod lengths and diameters and the ligand type and length are varied, it should be possible to learn a great deal about the intrinsic optical and electrical characteristics of the nanocrystals.

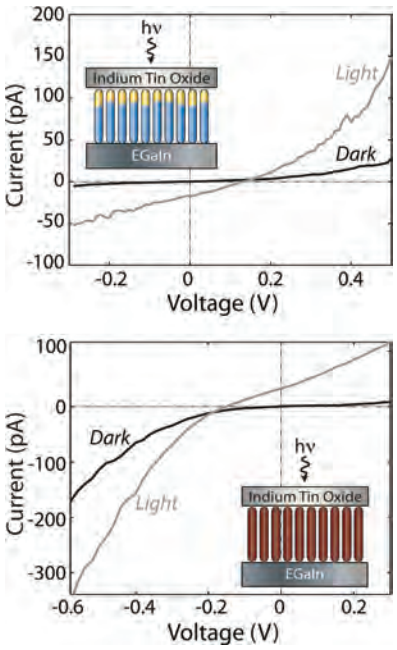

Figure 4. Current–voltage plot: Photovoltaic effect demonstrated in (top) a CdS–Cu_2S heterojunction and (bottom) a PbS Schottky nanodiode array.

We have presented a method for achieving a finely tunable compositional and electrical architecture using colloidal nanorods. Perpendicular self-assembly and in-film cation exchange enable the precise formation of a single-crystal epitaxial heterojunction in each oriented nanorod and can be used with a variety of chemical compositions. This advance may allow the production of inexpensive solution-processed photocatalysts, sensors, and optoelectronics. On the fundamental side, this architecture may

enable better understanding of charge transport longitudinally through nanorods (without any interparticle hops) and illuminate unique characteristics of devices at the few nanometer scale.

METHODS

Sample Preparation. Colloidal CdS nanorods were synthesized and self-assembled as reported elsewhere.[5] Briefly, nanorods were synthesized air-free with a CdO precursor in trioctylphosphine oxide and octadecylphosphonic acid. Nanorods were stored air-free, and colloidal concentrations were measured by UV−vis absorption calibrated with inductively coupled plasma mass spectrometry. With a controlled evaporation rate (<1 mm/min meniscus speed across a slightly tilted substrate), an elevated temperature (55 °C), an appropriate substrate (for example, silicon nitride), and a size-monodisperse sample, the nanorods oriented vertically.[5] The volume of nanorod solution needed for monolayer self-assembly was calculated by substrate area, assuming a 50% areal fill factor due to the long organic ligands on the nanorods. Substrates on which nanorods were to be aligned (Si_3N_4 for RBS measurements; 150 nm 20 Ω/square ITO on glass for electrical measurements) were cleaned by sequential sonication in water, toluene, isopropyl alcohol, and acetone, followed by an oxygen plasma etch. This cleaning procedure was performed to reduce the friction between the solvent meniscus and substrate, in an effort to avoid any stick−slip behavior that would be detrimental to film smoothness. Dried nanorod assemblies were cation exchanged air-free by soaking substrates in an anhydrous methanolic solution of (to go from CdS to Cu_2S) ∼0.1 mM tetrakis(acetonitrile)copper(I) hexafluorophosphate ($[MeCN]_4Cu^IPF_6$) or (to go from Cu_2S to PbS) ∼0.1 mM lead acetate and ∼0.1 mM trioctylphosphine. Cation exchange reactions were assumed to go to completion, so the exact amount of cation salt to be added could be calculated for the desired degree of exchange. After ∼12 h (to ensure reaction completion), substrates were removed from the cation solution and dipped in a vial of neat methanol. Cation exchange from CdS to Cu_2S was manifested by a change in film color from yellow to light brown. After cation exchange was complete, films were generally kept air-free and moisture-free, although these conditions may not be critical.

Electron Microscopy. SEM images were taken with a Zeiss Gemini Ultra-55 analytical scanning electron microscope at an accelerating voltage of 3 keV. EFTEM images were taken on a JEOL 2100F operated at 120 keV equipped with Gatan Tridiem imaging spectrometer. HRTEM images were taken on an FEI monochromated F20 UT Tecnai microscope operated at 200 keV. CdS wurztite simulation was performed using MacTempas.

Compositional Analysis. Rutherford backscattering data were taken with a 2.5 MeV Van de Graaff accelerator. The spectra were taken using a 2 MeV He^+ ion beam with a Si surface barrier detector at 165° with respect to the incident beam. The samples were tilted by 50° in order to improve depth resolution. The spectra were analyzed using the RUMP software package.

Energy-dispersive X-ray spectroscopy (EDS) was taken on a Zeiss Gemini Ultra-55 analytical scanning electron microscope (accelerating voltage 7 keV) with an EDAX EDS detector with Genesis software. A range of spot sizes and locations on film were measured before concluding compositional analysis and to confirm uniformity. Acquisition times were a few minutes. During EDS analysis, the quality of film and nanorod assembly were verified.

Electrical Characterization. All electrical measurements were taken in an argon glovebox. Current−voltage measurements were taken using a Keithly 236 source measurement unit and a probe station. A droplet of EGaIn (<1 mm diameter) was placed on top of the film and contacted with the "high" probe tip. Contact was made to the ITO by scraping off a small area of aligned rods and smearing indium onto this area for easy contact by the "low" probe. EGaIn contact areas were monitored with a 100× side-view camera. Multiple locations on each device were measured, and representative data were selected. AM1.5G illumination was provided by an Oriel 91160 300 W Xe solar simulator and was directed upward through a quartz window on the floor of the glovebox, on top of which the sample rested, nanorod film facing up.

Acknowledgment. We gratefully acknowledge P.K. Jain, B. Sadtler, J. Urban, D. Milliron, and E. Rabani for helpful discussions and critical review of the manuscript. We thank K.M. Yu for RBS data, and M.V.P. Altoe and S. Aloni for EFTEM data. SEM, EDS, and EFTEM were performed at the Molecular Foundry, Lawrence Berkeley National Laboratory (LBNL), and were supported by the Office of Science, Office of Basic Energy Sciences, Scientific User Facilities Division, of the U.S. Department of Energy under Contract No. DE-AC02-05CH11231. HRTEM was performed at the National Center for Electron Microscopy at LBNL. Work summarized in Figure 2 was funded by the Helios Solar Energy Research Center, which is supported by the Director, Office of Science, Office of Basic Energy Sciences of the U.S. Department of Energy under Contract No. DE-AC02-05CH11231. Work summarized in Figures 3 and 4 was supported by Director, Office of Science, Office of Basic Energy Sciences, of the United States Department of Energy under Contract No. DE-AC02-05CH11231 on the Inorganic/Organic Nanocomposites NSET Program, KC3104. J.B.R. and S.L.S. performed electrical measurements and were supported by National Science Foundation Graduate Student Fellowships. An Intel Fellowship supported the research on heterojunction formation (J.B.R.).

Supporting Information Available: Synthetic and self-assembly details. Rutherford backscattering, secondary ion mass spectrometry, and energy-dispersive X-ray spectroscopy methods and data. Details on electrical contacting method. This material is available free of charge *via* the Internet at http://pubs.acs.org.

REFERENCES AND NOTES

1. Talapin, D. V.; Shevchenko, E. V.; Murray, C. B.; Kornowski, A.; Forster, S.; Weller, H. CdSe and CdSe/CdS Nanorod Solids. *J. Am. Chem. Soc.* **2004,** *126*, 12984–12988.
2. Ryan, K. M.; Mastroianni, A.; Stancil, K. A.; Liu, H. T.; Alivisatos, A. P. Electric-Field-Assisted Assembly of Perpendicularly Oriented Nanorod Superlattices. *Nano Lett.* **2006,** *6*, 1479–1482.
3. Carbone, L.; Nobile, C.; De Giorgi, M.; Sala, F. D.; Morello, G.; Pompa, P.; Hytch, M.; Snoeck, E.; Fiore, A.; Franchini, I. R.; *et al.* Synthesis and Micrometer-Scale Assembly of Colloidal CdSe/CdS Nanorods Prepared by a Seeded Growth Approach. *Nano Lett.* **2007,** *7*, 2942–2950.
4. Gupta, S.; Zhang, Q. L.; Emrick, T.; Russell, T. P. "Self-Corralling" Nanorods under an Applied Electric Field. *Nano Lett.* **2006,** *6*, 2066–2069.
5. Baker, J. L.; Widmer-Cooper, A.; Toney, M. F.; Geissler, P. L.; Alivisatos, A. P. Device-Scale Perpendicular Alignment of Colloidal Nanorods. *Nano Lett.* **2010,** *10*, 195–201.
6. Sadtler, B.; Demchenko, D. O.; Zheng, H.; Hughes, S. M.; Merkle, M. G.; Dahmen, U.; Wang, L. W.; Alivisatos, A. P. Selective Facet Reactivity During Cation Exchange in Cadmium Sulfide Nanorods. *J. Am. Chem. Soc.* **2009,** *131*, 5285–5293.
7. Sullivan, G. A. Diffusion and Solubility of Cu in Cds Single Crystals. *Phys. Rev.* **1969,** *184*, 796–805.
8. Macdonald, F.; Lide, D. R. CRC Handbook of Chemistry and Physics. *Abstracts of Papers*; American Chemical Society: Washington, DC, 2003; Vol. 225, pp U552−U552.
9. Boer, K. W. The Cds/Cu_2S Solar Cell. *J. Cryst. Growth* **1982,** *59*, 111–120.

10. Pfisterer, F. The Wet-Topotaxial Process of Junction Formation and Surface Treatments of Cu_2S-CdS Thin-Film Solar Cells. *Thin Solid Films* **2003,** *431*, 470–476.
11. Robinson, R. D.; Sadtler, B.; Demchenko, D. O.; Erdonmez, C. K.; Wang, L. W.; Alivisatos, A. P. Spontaneous Superlattice Formation in Nanorods through Partial Cation Exchange. *Science* **2007,** *317*, 355–358.
12. Son, D. H.; Hughes, S. M.; Yin, Y. D.; Alivisatos, A. P. Cation Exchange Reactions in Ionic Nanocrystals. *Science* **2004,** *306*, 1009–1012.
13. Dloczik, L.; Koenenkamp, R. Nanostructured Metal Sulfide Surfaces by Ion Exchange Processes. *J. Solid State Electrochem.* **2004,** *8*, 142–146.
14. Luther, J. M.; Zheng, H. M.; Sadtler, B.; Alivisatos, A. P. Synthesis of PbS Nanorods and Other Ionic Nanocrystals of Complex Morphology by Sequential Cation Exchange Reactions. *J. Am. Chem. Soc.* **2009,** *131*, 16851–16857.
15. Dorn, A.; Allen, P. M.; Harris, D. K.; Bawendi, M. G. *In Situ* Electrical Monitoring of Cation Exchange in Nanowires. *Nano Lett.* **2010,** *10*, 3948–3951.
16. Song, J. H.; Messer, B.; Wu, Y. Y.; Kind, H.; Yang, P. D. MMo_3Se_3 (M = Li^+, Na^+, Rb^+, Cs^+, NMe^{4+}) Nanowire Formation *via* Cation Exchange in Organic Solution. *J. Am. Chem. Soc.* **2001,** *123*, 9714–9715.
17. Luther, J. M.; Law, M.; Beard, M. C.; Song, Q.; Reese, M. O.; Ellingson, R. J.; Nozik, A. J. Schottky Solar Cells Based on Colloidal Nanocrystal Films. *Nano Lett.* **2008,** *8*, 3488–3492.
18. Cui, Y.; Duan, X. F.; Hu, J. T.; Lieber, C. M. Doping and Electrical Transport in Silicon Nanowires. *J. Phys. Chem. B* **2000,** *104*, 5213–5216.
19. Trudeau, P. E.; Sheldon, M.; Altoe, V.; Alivisatos, A. P. Electrical Contacts to Individual Colloidal Semiconductor Nanorods. *Nano Lett.* **2008,** *8*, 1936–1939.
20. Bernede, J. C. Polarized Memory Switching in MIS Thin-Films. *Thin Solid Films* **1981,** *81*, 155–160.
21. Chiechi, R. C.; Weiss, E. A.; Dickey, M. D.; Whitesides, G. M. Eutectic Gallium−Indium (EGaIn): A Moldable Liquid Metal for Electrical Characterization of Self-Assembled Monolayers. *Angew. Chem., Int. Ed.* **2008,** *47*, 142–144.
22. Meng, X.; Lu, Y.; Yang, B.; Yi, G.; Jia, J. Fabrication and Photoelectrochemical Characteristics of the Patterned CdS Microarrays on Indium Tin Oxide Substrates. *ACS Appl. Mater. Interfaces* **2010,** *2*, 3467–3472.
23. Finlayson, M. F.; Wheeler, B. L.; Kakuta, N.; Park, K. H.; Bard, A. J.; Campion, A.; Fox, M. A.; Webber, S. E.; White, J. M. Determination of Flat-Band Position of Cds Crystals, Films, and Powders by Photocurrent and Impedance Techniques, Photoredox Reaction Mediated by Intragap States. *J. Phys. Chem.* **1985,** *89*, 5676–5681.
24. Reynolds, D. C.; Leies, G.; Antes, L. L.; Marburger, R. E. Photovoltaic Effect in Cadmium Sulfide. *Phys. Rev.* **1954,** *96*, 533–534.
25. Leon, M.; Terao, N.; Rueda, F. Phase-Transitions in Cuprous Sulfide Evaporated Thin-Films. *J. Mater. Sci.* **1984,** *19*, 113–120.
26. Yu, A. Y. C. Electron Tunneling and Contact Resistance of Metal−Silicon Contact Barriers. *Solid-State Electron.* **1970,** *13*, 239.
27. Johnston, K. W.; Pattantyus-Abraham, A. G.; Clifford, J. P.; Myrskog, S. H.; Hoogland, S.; Shukla, H.; Klem, J. D.; Levina, L.; Sargent, E. H. Efficient Schottky Quantum Dot Photovoltaics: The Roles of Depletion, Drift, and Diffusion. *Appl. Phys. Lett.* **2008,** *92*, 15115.
28. Huynh, W. U.; Dittmer, J. J.; Alivisatos, A. P. Hybrid Nanorod−Polymer Solar Cells. *Science* **2002,** *295*, 2425–2427.
29. Brandhorst, H. W. J. In *E-4722*; 1-17 National Aeronautics and Space Administration, 1969.
30. Rothwarf, A. The Cds-Cu_2S Solar Cell: Basic Operation and Anomalous Effects. *Sol. Cells* **1980,** *2*, 115–140.
31. Stanley, A. G. Cadmium Sulfide Solar Cells. *Appl. Solid State Sci.* **1975,** *5*, 251.
32. Nelson, J. *The Physics of Solar Cells*; Imperial College Press: London, 2003.
33. Fahrenbruch, A.; Bube, R. H. Heat-Treatment Effects in Cu_2S-CdS Heterojunction Photovoltaic Cells. *J. Appl. Phys.* **1974,** *45*, 1264–1275.